JOURNAL OF GEOPHYSICAL RESEARCH, VOL. 92, NO. A8, PAGES 8579–8593, AUGUST 1, 1987

The Emission of Narrow-Band Jovian Kilometric Radiation

S. F. FUNG

ORI, Inc., Landover, Maryland

K. PAPADOPOULOS

Astronomy Program, University of Maryland, College Park

A model based on the nonlinear coupling of electrostatic plasma waves is proposed to explain the emission of the narrow-band Jovian kilometric radiation (nKOM) observed by the Voyager spacecraft. it is shown that upper-hybrid branch electrostatic waves propagating through the inhomogeneities in the outer periphery of the Io plasma torus can attain the proper geometry for localized upconversion interactions leading to pump depletion. Plasma waves propagating into a weak density gradient (increasing ω_p/Ω_e) and reflected at the critical layer ($\omega_L = \omega_p$), interact with the incident waves leading to the electromagnetic emission at $2\omega_{UH}$, which is beamed at large angles with respect to the background magnetic field. In general, both *L-O* and *R-X* mode waves can be generated. The observed power and net polarization (*L-O*) are consistent with pump depletion of electrostatic waves at a level of ~ 10 mV/m. A possible excitation mechanism for the electrostatic waves is also discussed.

1. INTRODUCTION

It is well known from ground based observations that Jupiter radiates in the decimeter and decameter wavelengths [*Burke and Franklin*, 1955; *Sloanaker*, 1959; *McClain and Sloanaker*, 1959; *Carr et al.*, 1964; *Ellis*, 1965; *Zabriske*, 1970]. Recent satellite observations by the Pioneer spacecraft and later by the two celebrated Voyager encounters extended the known radio spectrum of Jupiter to hectometric and kilometric wavelengths [*Carr and Desch*, 1976; *Desch and Kaiser*, 1980; *Kaiser and Desch*, 1980]. The wealth of phenomenology of the Jovian magnetospheric radio emission has been comprehensively reviewed by *Carr et al.* [1983]. Unlike the well-studied decametric radiation (DAM), Jovian kilometric radiation (KOM) has received very little attention since its discovery [*Warwick et al.*, 1979*a*, *b*] till recently [*Fung*, 1985*a*, *b*; *Daigne and Leblanc*, 1986]. KOM is further complicated by the fact that it has two distinct components, the narrow-band (nKOM) and the broad-band (bKOM) emission. These two components are believed to originate from different parts of the Jovian magnetosphere [*Desch and Kaiser*, 1980; *Kaiser and Desch*, 1980; *Green and Gurnett*, 1980]; yet their similarities in frequences, powers, occurrence rate, and polarization suggest that their emission mechanisms may still be related.

In this paper, we consider the generation of the Jovan nKOM by upconversion interactions of electrostatic plasma waves. Such radiation mechanism has been proposed previously for the terrestrial auroral kilometric radiation [*Roux and Pellat*, 1979] and the Jovian DAM [*Goldstein et al.*, 1983]. In those cases, the interactions were assumed to be dipolelike (i.e., $k_{L1,2} \gg k_{em}$ and $\mathbf{k}_{L1} \simeq -\mathbf{k}_{L2}$), and the explicit satisfaction of the local electromagnetic dispersion relation in a magnetized plasma was not emphasized. This latter condition is crucial for determining the angles of propagation of the resulting radiation. Therefore, our results presented in the following are based on the detail satisfactions of the full dispersion relations of the interacting waves and the wave resonance conditions (equations (39) and (40)). Furthermore, a successful upconversion interaction requires that the group velocities of the interacting waves be ordered so that the pump wave packets would be propagating in opposite directions (colliding) when viewed in the frame of the high frequency product wave [*Kaup et al.*, 1979; *Fung*, 1985*b*]. This condition, generally ignored in the previous applications, is a stringent criterion controlling the possible coupling configurations and the upconversion efficiency of electrostatic to electromagnetic waves [*Fung*, 1985*b*]. The final distinction between the present and the previous models is that we consider the coupling of two electrostatic waves with mostly parallel instead of perpendicular wave vectors, in accordance to the optimal coupling configurations (see section 5.2).

We review first the pertinent observations of nKOM in the next section. We then identify, in section 3, the candidate pump waves amongst the electrostatic plasma waves observed in the Io plasma torus; a possible excitation mechanism for these waves will then be considered. In section 4, we develop the formalism and the equations that describe the coherent interaction between two electrostatic pump waves and an electromagnetic daughter wave. In section 5, we describe the coupling conditions and the source model for nKOM. The resulting polarization and power are compared to the observations in section 6.

2. NARROW-BAND JOVIAN KILOMETRIC RADIATION (nKOM)

2.1. *Observations*

The radiation characteristics of the nKOM are described in detail by *Kaiser and Desch* [1980] and *Carr et al.* [1983]. We summarize below the relevant nKOM observations.

The detection of nKOM was first noted by *Warwick et al.* [1979*b*], in their initial report on results from the Voyager 2 Jupiter encounter. Subsequent examinations of the Voyager 1 data also showed a distinct narrow-band component of the Jovian kilometric radiation. The nKOM events were detected between 60 and 150 kHz with bandwidth of 40–80 kHz. A typical frequency of maximum flux was around 100 kHz (see Figure 1). On the other hand, the bKOM events [*Desch and Kaiser*, 1980] can have a frequency of maximum flux around 70 kHz and a bandwidth of as high as 1 MHz. Typical nKOM events last for a few hours and are characterized by their

Paper number 6A8747.
0148-0227/87/006A-8747$05.00

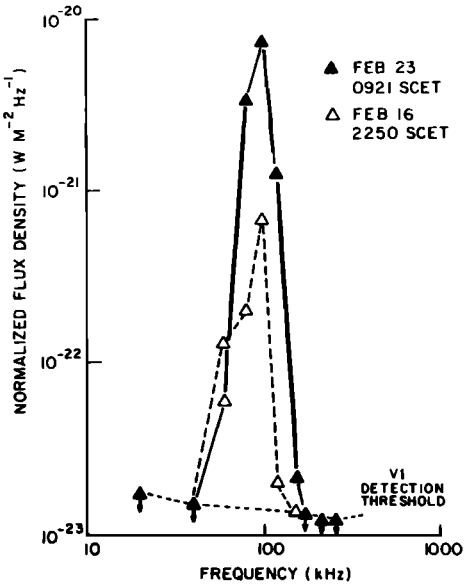

Fig. 1. A flux density spectrum for one of the stronger nKOM events observed on February 23, 1979. A more typical nKOM spectrum is exemplified by the event observed on February 16, 1979 [*Kaiser and Desch*, 1980].

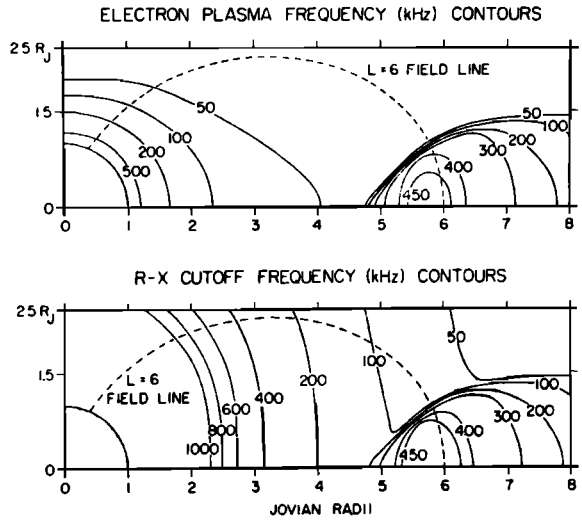

Fig. 2. The Jovian magnetosphere is shown as contours of the electron plasma frequency in kHz in the top panel. The bottom panel shows contours of the right-hand cutoff frequency $f_{R\text{-}X}$ in kilohertz [*Green and Gurnett*, 1980].

exceedingly smooth dynamic spectra. The nKOM bursts have slow build-up and decay, with little structure. The power of nKOM is comparable to that of their broadband counterpart (bKOM). If the radiation field were isotropic, the equivalent radiation power would be of the order of 10^9 W. A flux density spectrum normalized to an observation distance of 4 AU is shown in Figure 1.

There has been some confusion in the proper identification of the sense of polarization of the nKOM radiation. In the original paper by *Kaisr and Desch* [1980], the nKOM events were considered to be left-hand polarized. In a subsequent paper, *Kaiser and Desch* [1984] referred to unpublished work by Leblanc, who recognized that the exact orientation of the electrical plane of the PRA antennas during the Jupiter encounter trajectory would introduce a minus sign to the projection of the wave electric field onto the electrical plane. If this happened throughout the encounter, then the interpretation of the sense of polarization should be reversed [*Kaiser and Desch*, 1984]. However, it is now realized by Kaiser and Desch (private communication, 1985) that the original interpretation of the polarization was based on the strongest nKOM event observed by Voyager 2 near closest approach, which is not affected by the projection effect described before; thus the original identification of LH polarization for the nKOM radiation in the northern magnetic hemisphere remains correct (see also *Daigne and Leblanc* [1986]). Polarization reversals sometimes occur upon spacecraft crossings of the magnetospheric neutral sheet. However, there is also a large number of current sheet crossings concurring with nKOM events that show no polarization reversal.

A remarkable feature of the nKOM is that the same region must remain active for a long period of time. During a three-week interval, there were times when the nKOM was turned off for several planetary rotations. But when the nKOM reappeared, they continued on with the cycle of events as if there were no interruption of emission [*Kaiser and Desch*, 1980].

2.2. *Source Location*

Relatively strict limitations can be imposed on the source location of the nKOM emission. After plotting the system III longitudes of individual nKOM events from consecutive planetary rotations as a function of time, *Kaiser and Desch* [1980] discovered that the apparent nKOM source is rotating at a rate that is 3–5% slower than the planetary (system III) rotation rate. Based on the model of the radial breakdown in magnetospheric corotation [*Hill*, 1979, 1980], this amount of corotation lag occurs at a radial distance of 8–9 R_J, where R_J is Jupiter's planetary radius. Furthermore, from direct measurement of bulk motions of plasma ions in the Io plasma torus, *Bagenal and Sullivan* [1981] showed that the inner Jovian magnetosphere ceases to corotate strictly with Jupiter at distances greater than about 7.5 R_J. In particular, a less than 10% departure from corotational speed at distances between 7.5 R_J and 8.5 R_J provides a good agreement between ionic compositions and dynamics of different parts of the Io plasma torus at various radial distances.

Kaiser and Desch [1980] noted that Voyager 1 data show nKOM events down to a distance of 12 R_J from Jupiter. Perhaps due to refraction, no nKOM was detected near Voyager 1 closest approach (4.9 R_J). On the other hand, Voyager 2 data show nKOM events even at times near the Voyager 2 closest encounter at 10 R_J. These observations indicate that the nKOM source must lie in the periphery of the outer part of the Io plasma torus, between radial distances 7.5 R_J to 9 R_J, where the local characteristic frequencies (ω_p and Ω_e) can support radiation of about 100 kHz. Figure 2 shows the model contours of plasma frequencies and the *R-X* mode cutoff frequencies in the inner Jovian magnetosphere [*Green and Gurnett*, 1980]. It will be shown in section 3 that the nKOM source located between 7.5 and 9 R_J, near the outer periphery of the plasma torus where the plasma parameters are characterized by $2.3 < \omega_p/\Omega_e < 2.7$, is consistent with the observations.

3. Excitation of Electrostatic Cyclotron Harmonic Waves

In this section, we examine the possible excitation mechanism of the electrostatic plasma waves observed in the Io plasma torus. These waves may couple to produce electromagnetic radiation as they propagate into the resonance region, where the frequency and wave vector matching conditions ($\delta\omega = 0$, $\delta\mathbf{k} = 0$) are satisfied.

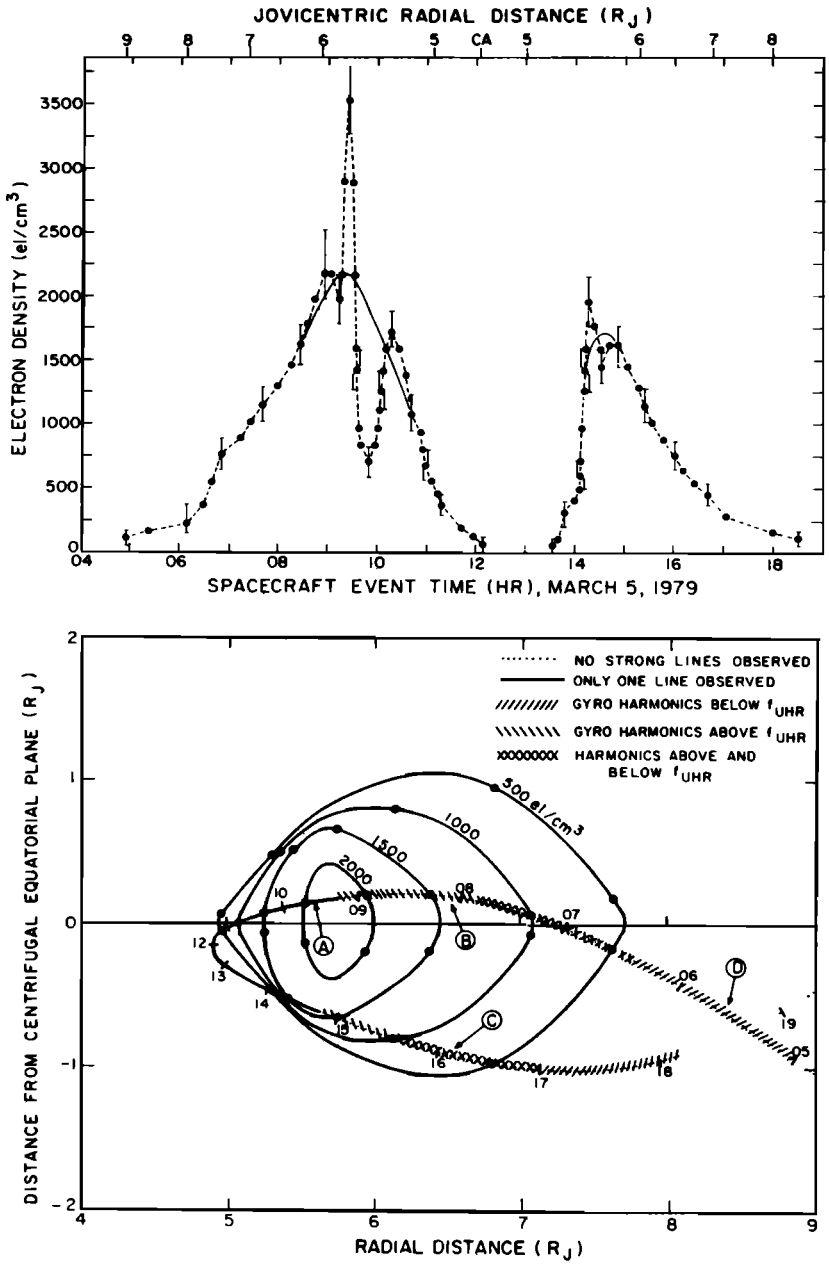

Fig. 3. (top) Plot of the density of the cold electron component of the Io plasma torus as a function of time derived from measurements of the cold upper hybrid resonance frequency and magnetometer measurements of the electron gyrofrequency. (bottom) A model of the average density distribution in meridional plane for the cold electron component of IPT. The projection of the Voyager 1 trajectory through the IPT is coded to indicate the locations at which various classes of plasma waves lines were detected. Spectra observed at the points marked A, B, C, and D are shown in Figure 4 [*Birmingham et al.*, 1981].

3.1. *Observations*

Electron cyclotron harmonic waves, much like those observed in the earth's magnetosphere, were detected throughout the Io plasma torus (IPT). These waves typically have frequencies falling in between integral harmonics of the local electron gyrofrequencies; thus, they are sometimes called electron half-harmonic waves. The characteristics of these waves observed in the Jovian magnetosphere are described in fair detail by *Kurth et al.* [1980*a*], *Scarf et al.* [1981], and *Birmingham et al.* [1981]. Figure 3 shows the meridional plane projection of the trajectory of Voyager 1 through the Io plasma torus. The direction of the trajectory is marked by the spacecraft event time (SCET) recorded onboard of the spacecraft. The types of harmonics present in the different portions of the trajectory, and hence different parts of the torus, are coded along the projected path. Four representative spectral density plots (Figure 4) corresponding to data taken at points A, B, C, and D (see Figure 3) show the distinct characteristics of various parts of the plasma torus [*Birmingham et al.*, 1981]. The upper-hybrid resonance is a dominant feature throughout the torus. However, the presence or absence of half-gyroharmonics above or below the local upper-hybrid resonance frequency $\omega_{UH} = (\omega_p^2 + \Omega_e^2)^{1/2}$, depends on the location in the torus. Within the cold component ($R \lesssim 5.6\ R_J$) of the torus [*Bagenal and Sullivan*, 1981], only the upper hybrid resonance is observed (Figure 4*a*). In the warm torus (5.6

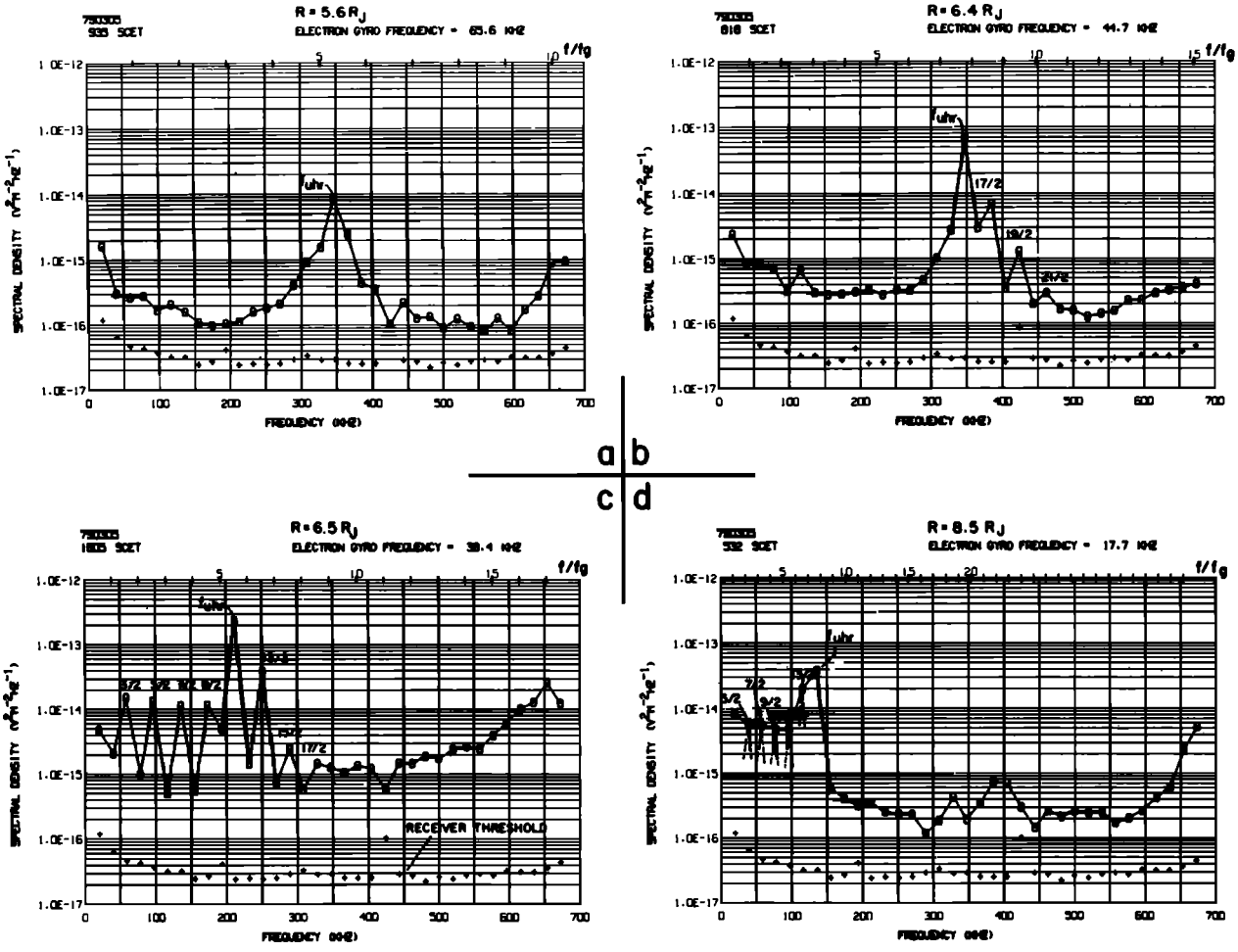

Fig. 4. Spectral density plots of gyroharmonics line emission in the IPT. Each plot is representative of a region in the torus characterized by a distinct line spectrum [*Birmingham et al.*, 1981].

$R_J \lesssim R \lesssim 7.5\ R_J$), both subharmonics and superharmonics are present (Figures 4*b* and 4*c*). At radial distances beyond about 7.5 R_J, only harmonics of frequencies below the upper hybrid resonance are detected (Figure 4*d*).

As we will see later, the maximum frequency for electrostatic waves in a cold, magnetized plasma is the upper hybrid resonance frequency. Therefore, the cold plasma model may be valid in the inner part ($R < 5.6\ R_J$) and the outer periphery ($R > 7.5\ R_J$) of the plasma torus. The existence of superharmonics in the warm torus indicates that finite temperature effects of the ambient plasma are not negligible [*Hubbard and Birmingham*, 1978; *Birmingham*, 1981]. Since the source region of the nKOM emission is located at distances greater than 7.5 R_J from Jupiter, where only harmonics of frequencies below the local ω_{UH} are observed, we consider that the cold plasma approximation is applicable for the consideration of the excitation of the electrostatic gyroharmonic waves.

3.2. *Excitation Mechanism*

The excitation mechanism of the terrestrial gyroharmonic waves has been studied quite extensively [*Hubbard and Birmingham*, 1978; *Ashour-Abdalla et al.*, 1979, and references therein]. It is generally believed that the electrostatic waves are generated by an unstable plasma distribution consisting of a dense, cold electron background component (<100 eV) and a hot, energetic electron component (~1 keV). Although a loss-cone type distribution [*Dory et al.*, 1965] is often assumed for the energetic hot component, which acts as the free energy source of the instability, the direct correspondence between the odd-half cyclotron harmonic emissions and such distribution function of the hot electrons has not been uniquely established [*Hasegawa*, 1975; *Kurth et al.*, 1980*b*; *Urrutia and Stenzel*, 1983].

Figure 5 shows the Voyager 1 measurements of the electron plasma distributions at three locations in the Io plasma torus region [*Scudder et al.*, 1981]. The presence of a cold background and a distinct suprathermal tail is evident. However, there is no indication of a positive slope in the distribution of the hot "halo" electrons. Moreover, a loss-cone in the torus region, near the magnetic equator, may be too weak to cause a significant wave growth. This renders the loss-cone type or beam type instabilities unlikely to be responsible for the generation of the cyclotron harmonic waves. A plasma distribution unstable to perturbations near the cyclotron half-harmonic frequencies and consistent with the observed particle spectra (Figure 5) is one with temperature anisotropy ($T_\perp > T_\parallel$). Although the temperature anisotropy required to produce the higher harmonic waves might be large (see equation (11)), it is compatible with the existence of a ring current near the magnetic equator [*Hasegawa*, 1975], at radial distances beyond 7 R_J. *Siscoe et al.* [1981] pointed out that the sharp drop in

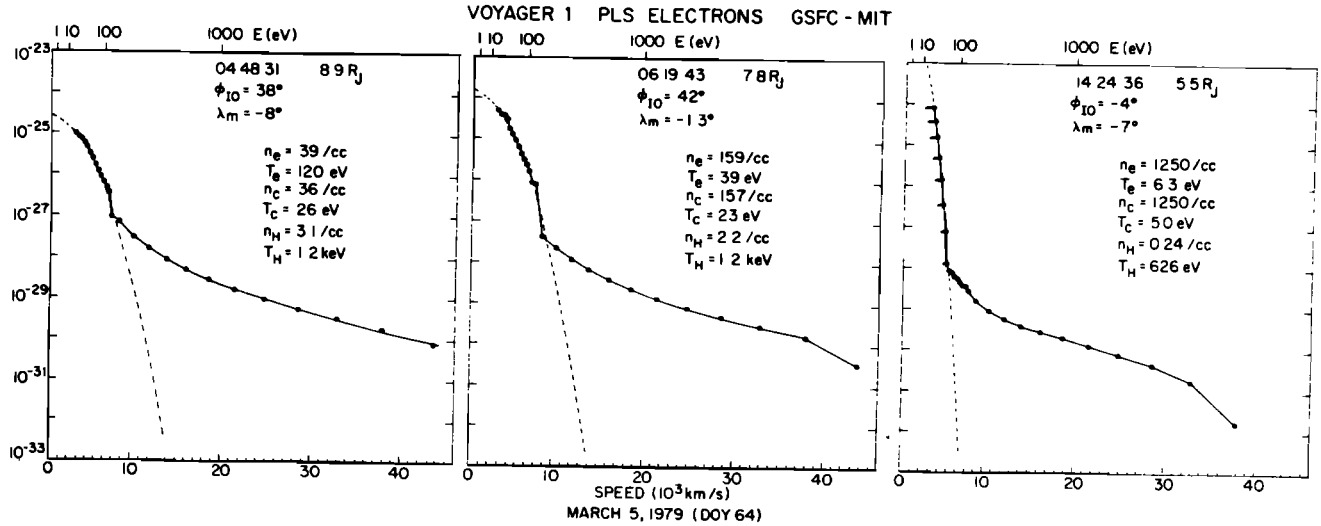

Fig. 5. Plots of the electron distribution function measured at three different times in the inner Jovian magnetosphere by Voyager 1 plasma science experiment. The measurement times, radial distance of spacecraft from Jupiter, system III longitude of spacecraft relative to Io, and dipole magnetic latitude of spacecraft are indicated. The connected points are data points, and the dashed lines are Maxwellian fits to the thermal background population of electrons [*Scudder et al.*, 1981].

density in the ramp region between 7 R_J and 8 R_J (Figure 6) can be attributed to the impoundment of the Io plasma torus due to an inwardly directed pressure of the ring current at its inner edge. If the current is confined to the equatorial region, a pronounced temperature anisotropy ($T_\perp \gg T_\parallel$) may result.

We consider next the excitation of the cyclotron half-harmonic waves due to the temperature anisotropy instability. We adopt a plasma model in which the ions are treated as an immobile, neutralizing background, and the electrons are found in two populations. The cold electron core can be represented by a delta function, while the hot halo component is given by a bi-Maxwellian distribution ($T_\perp \neq T_\parallel$); we thus have

$$f(v) = f_c(v) + f_H(v) \tag{1}$$

$$f_c(v) = \delta(v) \tag{2}$$

and

$$f_H(v) = \frac{\alpha}{(2\pi)^{3/2} v_{e\perp}{}^2 v_{e\parallel}} e^{(-v_\perp{}^2/2v_{e\perp}{}^2 - v_\parallel{}^2/2v_{e\parallel}{}^2)} \tag{3}$$

where α is the density ratio n_H/n_c, and $v_\perp$ and $v_{e\parallel}$ are the electron thermal speeds perpendicular and parallel to the ambient magnetic field, respectively.

The linear growth rate of kinetic plasma instabilities is generally given by [*Harris*, 1959; *Mikhailovskii*, 1974]

$$\gamma = -\frac{D_i}{(\partial D_r/\partial\omega)} \tag{4}$$

where the real part of the electrostatic dispersion function in a low β plasma is given by

$$D_r = 1 + \sum_s \frac{\omega_{ps}{}^2}{k^2} \sum_{n=-\infty}^{\infty} P \int dv \frac{J_n{}^2(k_\perp\rho)}{\omega - k_z v_z - n\Omega_s} \cdot \left[\frac{n\Omega_s}{v_\perp}\frac{\partial f}{\partial v_\perp} + k_z \frac{\partial f}{\partial v_z}\right] \tag{5}$$

and the imaginary part is

$$D_i = -\pi \sum_s \frac{\omega_{ps}{}^2}{k^2} \sum_{n=-\infty}^{\infty} \int dv\, J_n{}^2(k_\perp\rho)\left[\frac{n\Omega_s}{v_\perp}\frac{\partial f}{\partial v_\perp} + k_z \frac{\partial f}{\partial v_z}\right] \cdot \delta(\omega - k_z v_z - n\Omega_s) \tag{6}$$

with $k_\perp\rho = k_\perp v_\perp/\Omega_s$. The subscript s refers to the species of the plasma components.

It is straightforward to calculate the linear growth rate of the electrostatic waves by substituting our model distribution function (3) into (4) to obtain

$$\gamma(\omega, k) = -\alpha\left(\frac{\pi}{2}\right)^{1/2} \frac{\omega_p{}^2}{k^2|k_z|v_{e\parallel}{}^3} \frac{1}{(\partial D_r/\partial\omega)} \sum_{n=-\infty}^{\infty} I_n(z_\perp)e^{-z_\perp} \cdot \exp\left[-\frac{1}{2}\left(\frac{\omega - n\Omega_e}{k_z v_{e\parallel}}\right)^2\right]\left[\omega - n\Omega_e\left(1 - \frac{T_\parallel}{T_\perp}\right)\right] \tag{7}$$

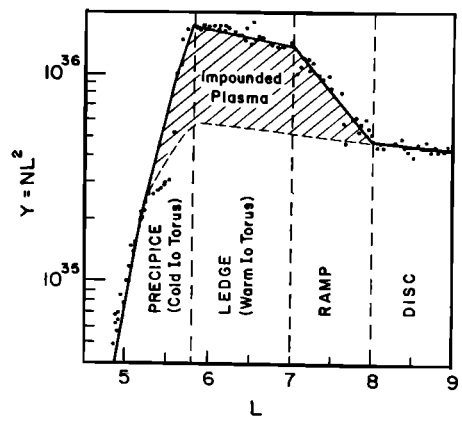

Fig. 6. Radial profile of the magnetic flux shell density $Y = NL^2$, where N is the number of ions in a flux shell per unit L. The presence of the ramp region signifies a substantially diminished level of diffusive activity. The origin of this feature is attributed to pressure gradient inhibition by a prominent precipitation edge of a ring current [*Siscoe et al.*, 1981].

where I_n are the nth-order modified Bessel functions with argument $z_\perp = (k_\perp v_{e\perp}/\Omega_e)^2$. We note that no instability will result from the $n = 0$ term. For instability, we require that $\gamma > 0$. Then, in the cold plasma limit ($|\omega - n\Omega_e| \gg k_z v_{e\parallel}$) and for a given harmonic number $n = m$ which leads to instability, we have an upper limit on the frequency of the unstable harmonic

$$\omega < m\Omega_e\left(1 - \frac{T_\parallel}{T_\perp}\right) \tag{8}$$

Furthermore, the most unstable wave must have frequency that is sufficiently close to the cyclotron harmonic so that its contribution to the growth rate (7) dominates over that of the other terms. This is satisfied if

$$\exp\left[-\frac{1}{2}\left(\frac{\omega - m\Omega_e}{k_z v_{e\parallel}}\right)^2\right] > \exp\left\{-\frac{1}{2}\left[\frac{\omega - (m-1)\Omega_e}{k_z v_{e\parallel}}\right]^2\right\} \tag{9}$$

It follows from (8) and (9) that the frequencies of the most unstable waves near the mth harmonic must fall within the range

$$(m - \tfrac{1}{2})\Omega_e < \omega < m\Omega_e\left(1 - \frac{T_\parallel}{T_\perp}\right) \tag{10}$$

This implies that an instability is possible ($\gamma > 0$) only when

$$\frac{T_\parallel}{T_\perp} < \frac{1}{2m} \qquad m = 1, 2, 3, \cdots \tag{11}$$

The minimum temperature anisotropy required for triggering the instability is $T_\parallel/T_\perp < 1/2$. When the cold plasma wave frequencies (see equation (45))

$$\omega_L{}^2 = \tfrac{1}{2}\{\omega_{UH}{}^2 = [\omega_{UH}{}^4 - 4\omega_p{}^2\Omega_e{}^2 \cos^2\theta_L]^{1/2}\} \tag{12}$$

fall within the unstable frequency range (10), electrostatic plasma waves are excited. If we now normalize all frequencies to the electron cyclotron frequency $\Omega_e = |e|B_0/(mc)$, we can see that the upper hybrid branch frequency, say ω_{L1}, is restricted to within the range

$$f_p < f_{L1} < (f_p{}^2 + 1)^{1/2} \tag{13}$$

where $f_p = \omega_p/\Omega_e$ and $f_{L1} = \omega_{L1}/\Omega_e$. In order to excite the upper hybrid mode in a cold plasma, the wave frequencies (13) must fall within the unstable range (10). The compatibility between (10) and (13) dictates that for a plasma characterized by a given ω_p/Ω_e and $T_\parallel/T_\perp$, only those waves with harmonic number m satisfying the inequality

$$[(m - \tfrac{1}{2})^2 - 1]^{1/2} < f_p < m\left(1 - \frac{T_\parallel}{T_\perp}\right) \tag{14}$$

will be driven unstable. Thus high harmonics are generated in the IPT, close to the magnetic or centrifugal equator where ω_p/Ω_e is large, whereas low harmonics are produced in regions of lower density and/or stronger magnetic field (see Figure 2).

Figure 3 shows the latitudinal and radial variations of electron density in the plasma torus region. At radial distances between 7.5 R_J and 9 R_J the plasma densities are high near the equator. The corresponding plasma frequencies ($\sim$142 kHz at 0600 SCET) are typically higher than the observed nKOM frequencies. We, therefore, conclude that the source of nKOM must be located near the outer periphery of the Io plasma torus, away from the magnetic (or centrifugal) equator.

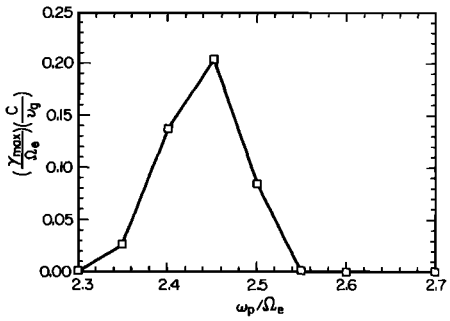

Fig. 7a. (Im $k)_{max} = (\gamma_{max}/\Omega_e)(c/v_g)$ against ω_p/Ω_e for $T_\parallel = 0.2$ kev, $T_\parallel/T_\perp = 0.1$, $\alpha = 10^{-2}$.

Assuming a dipole magnetic field, the electron gyrofrequencies in the source region near 8 R_J range between 20 and 25 kHz. This implies that the observed nKOM frequencies ($\sim$100 kHz) are about 5 times the local gyrofrequency at the source region. Thus the observed nKOM frequencies can result from the upconversion of two upper hybrid branch waves, each with $\omega_L \simeq 5/2\ \Omega_e$, generated in a region where the plasma parameters are given by (substituting $m = 3$ in equation (14))

$$2.3 < \frac{\omega_p}{\Omega_e} < 3\left(1 - \frac{T_\parallel}{T_\perp}\right) \tag{15}$$

with $T_\parallel/T_\perp < 1/6$. Figure 7a shows the maximum convective growth rate (Im $k)_{max} \simeq (\gamma/v_g)_{max}$ of the electrostatic upper-hybrid waves as a function of ω_p/Ω_e, calculated according to the temporal growth rate (7) and group velocity [*Goldstein et al.*, 1983; *Fung*, 1985*b*]. In our calculations, we adopted the following parameters: $\alpha = 10^{-2}$, $T_\parallel = 0.2$ keV, and $T_\parallel/T_\perp = 0.1$. It was found that the most unstable zone is near $2.4 \lesssim \omega_p/\Omega_e \lesssim 2.5$. Taking $\omega_p/\Omega_e = 2.45$, the normalized growth rate Im k/(Im k_{max}) as functions of k and θ are plotted in Figures 7b and 7c. The maximum growth rate (Im $k)_{max} = 0.2\ \Omega_e/c$ occurs for $kc/\Omega_e = 51$, $\omega/\Omega_e = 2.6413$, and $\theta = 80°$ (or 100°). The bandwidths in k, θ, and ω are given by the points where Im k/|Im $k|_{max} \sim 0.1$. We thus have $20 \lesssim kc/\Omega_e \lesssim 180$, $67 \lesssim \theta \lesssim 86$, and $2.6209 \lesssim \omega_L/\Omega_e \lesssim 2.6454$. In the next section we discuss how these electrostatic waves can take part in an upconversion process to produce radiation when they propagate into the resonance zone.

4. Three-Wave Interaction Equations and the Coupling Coefficient

The equations that describe coherent three-wave interaction processes can be derived by the standard multiple timescale analysis in which the wave profiles are separated into a fast

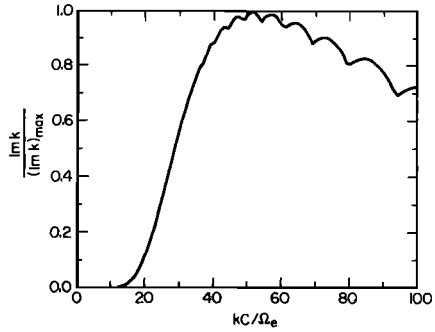

Fig. 7b. Im k/(Im k)max vs. kc/Ω_e.

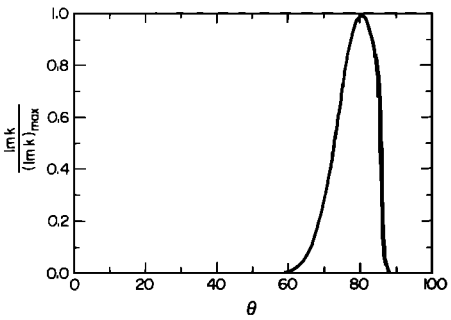

Fig. 7c. Im k/(Im k)max vs. θ.

oscillating carrier wave and a slowly modulated envelope [*Davidson*, 1972; *Hasegawa*, 1975]. The wave amplitudes form the envelope profile and are modulated by the coupling process. The resulting set of equations, derived in the weak turbulence regime, contains only quadratic nonlinearities. It is assumed that, apart from the coupling nonlinearity, the linear propagation properties of these waves are unchanged, and the plasma in which these waves propagate retains its linear dielectric properties.

Let $\mathbf{E}_j$ and $\mathbf{E}_k$ be the electric field vectors of two low-frequency electrostatic pump waves, and $\mathbf{E}_i$ be that of a high frequency electromagnetic wave with $\omega_i > \omega_j$, ω_k. If we write the magnitudes of the wave electric field vectors E_μ in terms of their envelope profiles and carrier waves, and generalize the propagation vectors to incorporate any linear (WKB-like) inhomogeneity of the plasma [*Rosenbluth*, 1972], i.e.,

$$E_\mu(\mathbf{r}, t) = \varepsilon_\mu(\mathbf{r}, t) \exp\left(-i\omega_\mu(\mathbf{k}_\mu)t + i\int_0^{\mathbf{r}} \mathbf{k}_\mu(\tilde{\mathbf{r}}) \cdot d\tilde{\mathbf{r}}\right) \tag{16}$$

the three-wave interaction equations become [*Fung*, 1985*b*]

$$\left(\frac{\partial}{\partial t} + \mathbf{v}_i \cdot \nabla\right)\varepsilon_i(\mathbf{r}, t) = K_i\varepsilon_j\varepsilon_k \exp\left(i\delta\omega t - i\int_0^{\mathbf{r}} \delta\mathbf{k} \cdot d\tilde{\mathbf{r}}\right) \tag{17}$$

$$\left(\frac{\partial}{\partial t} + \mathbf{v}_j \cdot \nabla\right)\varepsilon_j(\mathbf{r}, t) = K_j^*\varepsilon_i\varepsilon_k^* \exp\left(-i\delta\omega t + i\int_0^{\mathbf{r}} \delta\mathbf{k} \cdot d\tilde{\mathbf{r}}\right) \tag{18}$$

$$\left(\frac{\partial}{\partial t} + \mathbf{v}_k \cdot \nabla\right)\varepsilon_k(\mathbf{r}, t) = K_k^*\varepsilon_i\varepsilon_j^* \exp\left(-i\delta\omega t + i\int_0^{\mathbf{r}} \delta\mathbf{k} \cdot d\tilde{\mathbf{r}}\right) \tag{19}$$

where

$$\mathbf{v}_\mu = -\left.\frac{\partial D_\mu/\partial\mathbf{k}}{\partial D_\mu/\partial\omega}\right|_{\omega_\mu(\mathbf{k}_\mu)} \tag{20}$$

are the group velocities of the interacting waves with linear dispersion relations given by $D_\mu = \det \mathbf{D}_\mu = 0$ ($\mu = i, j, k$); K_μ are the coupling coefficients, which for a conservative system can be symmetrized to a unique quantity; $\delta\omega$ and $\delta\mathbf{k}$ are the mismatches in frequency and wave number, respectively. In this representation, the origin $\tilde{\mathbf{r}} = 0$ is chosen to be the resonance point where the frequency mismatch

$$\delta\omega = \omega_i - \omega_j - \omega_k \tag{21}$$

and wave number mismatch

$$\delta\mathbf{k} = \mathbf{k}_i(\tilde{\mathbf{r}}) - \mathbf{k}_j(\tilde{\mathbf{r}}) - \mathbf{k}_k(\tilde{\mathbf{r}}) \tag{22}$$

vanish (i.e., $\delta\omega = 0$ and $\delta\mathbf{k} = 0$ at $\tilde{\mathbf{r}} = 0$).

In the vicinity of the resonance point, we can normalize the wave amplitudes to the action densities of the waves. In the limit that the growth or damping rates of the plasma waves are negligibly small, the three-wave equations can be symmetrized, and a unique coupling coefficient can be defined. The energy density carried by a wave in a plasma is given by [*Landau and Lifshitz*, 1960; *Stix*, 1962]

$$W_\mu = \mathbf{E}_\mu^* \cdot \frac{\partial}{\partial\omega}(\omega\mathbf{D}_\mu) \cdot \mathbf{E}_\mu\Big|_{\omega_\mu(\mathbf{k}_\mu)} \tag{23}$$

or, equivalently,

$$W_\mu = p_\mu\omega_\mu a_\mu^* a_\mu \tag{24}$$

where p is the sign (plus or minus) of the wave energy density determined by the derivative in (23), ω_μ is the wave frequency, and $a_\mu^* a_\mu$ is the action density. The normalized amplitude a_μ of the electrostatic pump waves are given by

$$a_{j,k} = \left|\frac{\partial D_{j,k}}{\partial\omega}\right|_{\omega_{j,k}}^{1/2} \varepsilon_{j,k} \tag{25}$$

For the electromagnetic wave, however, one must account for the fact that the wave electric field components are coupled by the dispersion tensor $\mathbf{D}_{em} = \mathbf{D}_i$; and the wave energy density in the form of (24) must be expressed in terms of one component of the electric field [*Fung*, 1985*b*]. We then have

$$a_i = \sigma_i\left|\alpha_i \frac{\partial D_i}{\partial\omega}\right|_{\omega_i}^{1/2} \varepsilon_i \tag{26}$$

where ε_i can be any one of the electromagnetic wave electric field components ε_x, ε_y, or ε_z; correspondingly, $\sigma_i = \sigma_{x,y,z}$ ($\sigma_x = 1$, $\sigma_y = \pm i$, and $\sigma_z = -1$); and $\alpha_i = \alpha_{x,y,z}$ with

$$\alpha_x = \frac{1}{(\varepsilon_3 - n_i^2 \sin^2\theta_i)(\varepsilon_1 - n_i^2)} \tag{27}$$

$$\alpha_y = \frac{(\varepsilon_1 - n_i^2)}{\varepsilon_2^2(\varepsilon_3 - n_i^2 \sin^2\theta_i)} \tag{28}$$

and

$$\alpha_z = \frac{\varepsilon_3 - n_i^2 \sin^2\theta_i}{(\varepsilon_1 - n_i^2)n_i^4 \sin^2\theta_i \cos^2\theta_i} \tag{29}$$

The plus or minus sign of σ_y corresponds to the polarization of *L-O* or *R-X* mode of propagation, respectively. In the cold plasma limit, the refractive index n_i and the dielectric elements ε_1, ε_2, and ε_3 are given by [*Stix*, 1962]

$$n_i^2 = \underset{R\text{-}X}{n_{L\text{-}O}}^2 = 1 - \frac{2\alpha(1-\alpha)}{2(1-\alpha) - \beta\sin^2\theta_i \pm \beta^{1/2}\Delta} \tag{30}$$

with

$$\Delta = [\beta\sin^4\theta_i + 4(1-\alpha)^2\cos^2\theta_i]^{1/2}$$

$$\varepsilon_1 = 1 - \alpha/(1-\beta) \qquad \varepsilon_2 = \frac{\alpha\beta^{1/2}}{1-\beta} \qquad \varepsilon_3 = 1 - \alpha \tag{31}$$

where $\alpha^{1/2} = \omega_{pe}/\omega_i$ and $\beta^{1/2} = |\Omega_e|/\omega_i$ are the normalized electron plasma and cyclotron frequencies; θ_i is the wave normal angle with respect to the background magnetic field $\mathbf{B}_0 = B_0\mathbf{e}_z$. Using (25) and (26), the steady state three-wave interaction equations in two dimensions can be written as

$$\left(v_{ix}\frac{\partial}{\partial x} + v_{iz}\frac{\partial}{\partial z}\right)a_i = p_i K a_j a_k \tag{32}$$

$$\left(v_{jx}\frac{\partial}{\partial x}+v_{jz}\frac{\partial}{\partial z}\right)a_j=-p_jK^*a_ia_k^* \tag{33}$$

$$\left(v_{kx}\frac{\partial}{\partial x}+v_{kz}\frac{\partial}{\partial z}\right)a_k=-p_kK^*a_ia_j^* \tag{34}$$

where K is the symmetrized coupling coefficient,

$$K=-\frac{4\pi p_i}{\omega_iE_jE_k}\frac{|(\varepsilon_1-n_i^2)(\varepsilon_3-n_i^2\sin^2\theta_i)|^{1/2}}{|\partial D_i/\partial\omega|_{\omega_i}^{1/2}|\partial D_j/\partial\omega|_{\omega_j}^{1/2}|\partial D_k/\partial\omega|_{\omega_k}^{1/2}}\mathbf{k}_i\cdot\mathbf{J}_i^{NL} \tag{35}$$

with

$$\mathbf{k}_i=\mathbf{e}_x-\frac{i\varepsilon_2}{(\varepsilon_1-n_i^2)}\mathbf{e}_y-\frac{n_i^2\sin\theta_i\cos\theta_i}{\varepsilon_3-n_i^2\sin^2\theta_i}\mathbf{e}_z \tag{36}$$

as the polarization vector of $\mathbf{E}_i$ [*Akhiezer et al.*, 1975], and $\mathbf{J}_i^{NL}$ as the nonlinear current density driven by the coupling of the two electrostatic pump waves.

To calculate the nonlinear current, we follow *Roux and Pellat* [1979] and *Goldstein et al.* [1983]. Details of the calculations are given in *Fung* [1985*b*]. Apart from the assumption of axial symmetry about the background magnetic field $\mathbf{B}_0=B_0\mathbf{e}_z$, no approximations have been made of the coupling geometry. In the limit of cold magnetized plasma, the linearized density and velocity perturbations due to the two electrostatic waves ($\mathbf{E}_j$ and $\mathbf{E}_k$) propagating in the $x-z$ plane, i.e., $\mathbf{k}_{j,k}=k_x\mathbf{e}_x+k_z\mathbf{e}_z$, can be ascertained from the fluid equations. The resonance conditions $\delta\omega=0$ and $\delta\mathbf{k}=0$ ((21) and (22)) imply that the Fourier-transformed nonlinear current density $\mathbf{J}_i^{NL}$ is given by

$$\mathbf{J}^{NL}(\omega_i,\mathbf{k}_i)=-\frac{e}{2}[n_j(\omega_j,\mathbf{k}_j)\mathbf{v}_k(\omega_k,\mathbf{k}_k)+n_k(\omega_k,\mathbf{k}_k)\mathbf{v}_j(\omega_j,\mathbf{k}_j)]-en_0\,\mathbf{V}_p(\omega_i,\mathbf{k}_i) \tag{37}$$

where

$$\mathbf{V}_p(\omega_i,\mathbf{k}_i)=\frac{1}{2\omega_i}[(\mathbf{v}_j\cdot\mathbf{k}_k)\mathbf{v}_k+(\mathbf{v}_k\cdot\mathbf{k}_j)\mathbf{v}_j]$$

is the velocity perturbation due to the ponderomotive forces. As $\mathbf{E}_j$ and $\mathbf{E}_k$ are electrostatic, there is no Lorentz term. Normalizing the wave frequencies by the electron cyclotron frequency Ω_e, we obtain the nonlinear current density $\mathbf{J}_i^{NL}(\omega_i,\mathbf{k}_i)$ [*Fung*, 1985*b*]:

$$\mathbf{J}_i^{NL}(\omega_i,\mathbf{k}_i)=\frac{eE_jE_k}{8\pi m\Omega_e(f_j^2-1)(1-f_k^2)}\left(\frac{\omega_p}{\Omega_e}\right)^2\cdot[j_x^{NL}\mathbf{e}_x+j_y^{NL}\mathbf{e}_y+j_z^{NL}\mathbf{e}_z] \tag{38}$$

with

$$\begin{aligned}j_x^{NL}=&-\frac{k_jf_k}{f_j^2}(f_j^2-\cos^2\theta_j)\sin\theta_k-\frac{k_kf_j}{f_k^2}(f_k^2-\cos^2\theta_k)\sin\theta_j\\&-\frac{f_jf_k}{f_i}(k_k\sin\theta_k+k_j\sin\theta_j)\sin\theta_j\sin\theta_k\\&-\frac{\cos\theta_j\cos\theta_k}{f_if_jf_k}[(f_j^2-1)f_k^2k_k\sin\theta_k\\&-(1-f_k^2)f_j^2k_j\sin\theta_j]\end{aligned}$$

$$j_y^{NL}=-\frac{ik_j}{f_j^2}(f_j^2-\cos^2\theta_j)\sin\theta_k-\frac{ik_k}{f_k^2}(f_k^2-\cos^2\theta_k)\sin\theta_j$$

$$\begin{aligned}&-\frac{i\sin\theta_j\sin\theta_k}{f_i}(f_jk_k\sin\theta_k+f_kk_j\sin\theta_j)\\&-\frac{i\cos\theta_j\cos\theta_k}{f_i}\left[\frac{(f_j^2-1)k_k\sin\theta_k}{f_j}\right.\\&\left.-\frac{(1-f_k^2)k_j\sin\theta_j}{f_k}\right]\end{aligned}$$

and

$$\begin{aligned}j_z^{NL}=&\frac{(1-f_k^2)k_j\cos\theta_k}{f_kf_j^2}(f_j^2-\cos^2\theta_j)\\&-\frac{(f_j^2-1)k_k\cos\theta_j}{f_k^2f_j}(f_k^2-\cos^2\theta_k)\\&+\frac{\sin\theta_j\sin\theta_k}{f_if_jf_k}[(1-f_k^2)f_j^2k_k\cos\theta_k\\&-(f_j^2-1)f_k^2k_j\cos\theta_j]\\&+\frac{(f_j^2-1)(1-f_k^2)}{f_if_jf_k}(k_k\cos\theta_k+k_j\cos\theta_j)\cos\theta_j\cos\theta_k\end{aligned}$$

where $f=\omega/\Omega_e$. Since we have not distinguished the two electrostatic waves, our nonlinear current is general and symmetric upon interchanging of the subscripts j and k.

We should point out here that our derivations of the coupling equations (32)–(34) and the coupling coefficient (35) differs from the previous works [*Roux and Pellat*, 1979; *Goldstein et al.*, 1983] in that it properly takes into account of the polarization and action density of the electromagnetic wave (equations (23) and (26)).

5. Coupling Geometry and Source Model

In this section, we propose a source model for the nKOM emission of Jupiter. We demonstrate that configuration constraints for efficient upconversion coupling [*Fung*, 1985*b*] can be satisfied in the Io plasma torus. We first discuss the conditions that control the upconversion coupling configuration.

5.1. *Conditions for Coupling*

Resonant three-wave interaction cannot occur among an arbitrary triplet of waves. We list below the conditions which allow three-wave resonant interaction. (Subscripts 1 and 2 represent the electrostatic pump waves.)

The three-wave resonance conditions are

$$\omega_{em}=\omega_{L1}+\omega_{L2} \tag{39}$$

$$\mathbf{k}_{em}=\mathbf{k}_{L1}+\mathbf{k}_{L2} \tag{40}$$

For the electrostatic (pump) waves propagating in a cold magnetized plasma, the wave numbers $k_{L1,2}$ must satisfy the electrostatic approximation [*Stix*, 1962]:

$$k_D\gg k_{L1,2}>k_{\min} \tag{41}$$

where

$$k_{\min}^2=\frac{\omega_L^2}{c^2}|\varepsilon_{ij}|_{\max} \tag{42}$$

is the minimum wave number; $|\varepsilon_{ij}|_{\max}$ is the largest of the dielectric elements (31) computed by using the electrostatic wave frequencies; k_D is the Debye wave number. The first inequality in (41) is inherently satisfied by all plasma waves

and is consistent with the cold approximation. We have thus the following condition for the cold plasma:

$$\frac{\Omega_e}{ck_{L1,2}}\left(\frac{\omega_p}{\Omega_e}\right) \gg \frac{v_e}{c} \tag{43}$$

The satisfaction of the eigenmode dispersion relations,

$$D_\mu(\omega_\mu, \mathbf{k}_\mu) = 0 \tag{44}$$

of the interacting waves. The eigenmode frequencies of the electrostatic waves can be easily obtained from the electrostatic dispersion relation $D_{es} = 0$ [*Akhiezer et al.*, 1975], so that

$$\omega_L{}^2 = \tfrac{1}{2}\{\omega_{UH}{}^2 \pm [\omega_{UH}{}^4 - 4\omega_p{}^2\Omega_e{}^2 \cos^2\theta]^{1/2}\} \tag{45}$$

where $\omega_{UH} = (\omega_p{}^2 + \Omega_e{}^2)^{1/2}$ is the upper hybrid resonance frequency. The plus or minus sign in (45) corresponds to the upper or lower hybrid branch of magnetized electron plasma waves, respectively. The dispersion relation for the high frequency electromagnetic wave in a cold plasma can be written in the familiar form [*Allis et al.*, 1962; *Stix*, 1962]

$$An^4 - Bn^2 + C = 0 \tag{46}$$

where

$$A = \varepsilon_1 \sin^2\theta + \varepsilon_3 \cos^2\theta$$

$$B = (\varepsilon_1{}^2 - \varepsilon_2{}^2)\sin^2\theta + \varepsilon_1\varepsilon_3(1 + \cos^2\theta)$$

$$C = \varepsilon_3(\varepsilon_1{}^2 - \varepsilon_2{}^2)$$

The refractive indices $n^2 = n_\pm{}^2$ for R-$X(-)$ and L-$O(+)$ modes are given by (30).

For freely propagating electromagnetic waves, their frequencies must be above the respective mode cutoff frequencies ($\omega_{L\text{-}O}$ and $\omega_{R\text{-}X}$), i.e.,

$$\omega_{em} > \omega_{\substack{L\text{-}O \\ R\text{-}X}} \tag{47}$$

depending on the mode of propagation (L-O or R-X). Waves with frequencies higher than the cutoff frequencies will propagate freely in the medium. Contrastingly, waves with frequencies below the cutoff frequencies will be tapped and reflected at the cutoff ($n_\pm = 0$). The cutoff frequencies for the L-O and R-X modes can be obtained by setting $n = 0$ in (46) and solving $C = 0$. We then have

$$\omega_{L\text{-}O} = \omega_p \tag{48}$$

and

$$\omega_{R\text{-}X} = \tfrac{1}{2}[\Omega_e + (4\omega_p{}^2 + \Omega_e{}^2)^{1/2}] \tag{49}$$

For the occurrence of an upconversion interaction, it is required that the two pump wave packets be propagating in opposite directions when viewed in the frame of the high frequency wave packet. In a two-dimensional, steady state interaction described by (32) to (34), the ordering in group velocities becomes the ordering in the ratio of the components of the group velocities [*Kaup et al.*, 1979; *Fung*, 1985*b*], i.e.,

$$(C_j - C_i)(C_k - C_i) < 0 \tag{50}$$

where $C_\mu = (v_{gz}/v_{gx})_\mu$. For waves propagating in the $x - z$ plane, the group velocities can be computed directly according to (20); their analytic expressions are given in *Goldstein et al.* [1982] and *Fung* [1985*b*].

5.2. *Source Model*

Due to the relatively high equivalent isotropic power ($\sim 10^9$ W) and the narrow-band nature ($\Delta\omega < \omega$) of the nKOM, we consider the generation of the nKOM by the coherent (upconversion) interaction of two electrostatic electron gyroharmonic waves observed by *Birmingham et al.* [1981] in the Io plasma torus. Detailed description and the basis of our model have been given by *Fung* [1985*b*]. We outline here only the basic concepts involved.

The key notion in our model is to make use of the high conversion efficiencies associated with the depletion of the pump waves. This situation has been explored by *Roux and Pellat* [1979] for the case of the auroral kilometric radiation (AKR). By balancing the energy fluxes of the electrostatic and electromagnetic waves, they derived a pump depletion condition which is highly dependent on the inhomogeneity of the plasma. In this paper, we adopt the results obtained via the inverse scattering transform analysis of the full, steady state three-wave interaction equations (32)–(34) derived in section 4 [*Zakharov and Manakov*, 1976; *Kaup et al.*, 1979; *Fung*, 1985*b*]. It is found that the threshold condition for pump depletion is equivalent to that of soliton formation; and it is the same as the condition for the occurence of linear absolute parametric decay instability. It is also shown that when soliton solutions appear in the pump wave profiles, these solitons are transferred into the high frequency daughter wave, leading to the depletion of the pump waves. When the wave packet profiles are slowly varying functions (WKB-like), we can obtain the pump-depletion threshold for the upconversion (soliton-exchange) interaction, expressed in terms of the normalized pulse areas $A_{j,k}$ of the pump waves $\tilde{a}_j$ and $\tilde{a}_k$. We have defined the pulse area as

$$A_{j,k}(\tau) = \int_{-\infty}^{\infty} |q_{j,k}(z, \tau)|\, dz \tag{51}$$

where

$$|q_{j,k}(z, \tau)| = \frac{|K\tilde{a}_{j,k}(z, \tau)|}{[(C_{i,k} - C_j)(C_k - C_{j,i})]^{1/2}} \tag{52}$$

are the so-called scattering potentials. The C_μ in (52) are the ratio of the components of the group velocities as in (50); K is the coupling coefficient given by (35); $\tilde{a}_{j,k}$ are related to the wave amplitude profiles $a_{j,k}$ in (32)–(34), $a_{j,k} = (v_{ix}v_{k,jx})^{1/2}\tilde{a}_{j,k}$, such that (32)–(34) can be transformed to an equivalent one-dimensional (z)–temporal ($x \rightarrow \tau$) system by dividing through by the x components of the group velocities. The application of the inverse scattering transform analysis to this new system is straightforward [*Zakharov and Manakov*, 1976; *Kaup et al.*, 1979; *Fung*, 1985*b*].

For a quasi-classical (WKB) wave packet, the pump depletion threshold condition is

$$A_{j,k} \geq \frac{\pi}{2} \tag{53}$$

We can approximate (51) and (52) by

$$A \simeq Q\varepsilon L \tag{54}$$

where ε and L are the wave electric field amplitude and pulse length, respectively. The parameter Q characterizes the coupling process. Since the length of a wave packet is restricted by the system size (density scale length) L_n and the bandwidth Δk as dictated by the uncertainty principle [*Merzbacher*,

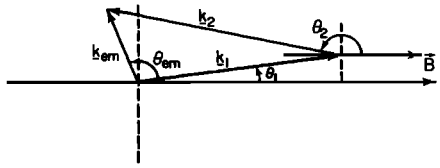

Fig. 8. Coupling configuration for the interaction of two upper hybrid branch waves ($\mathbf{k}_{L1}$ and $\mathbf{k}_{L2}$) and an electromagnetic wave ($\mathbf{k}_{em}$).

1970], L must be found within the range

$$L_n > L \gg \frac{1}{\Delta k} \tag{55}$$

Combining (53) and (54), we obtain the threshold amplitude for the occurrence of pump depletion or absolute instability, i.e.,

$$\varepsilon_{th} \simeq \frac{\pi}{2QL} \tag{56}$$

When the coupling conditions in section 5.1 are satisfied by the interacting waves, and the pump waves satisfy the soliton threshold ($\varepsilon \sim \varepsilon_{th}$), strong radiation can be produced.

According to *Fung* [1985*b*], the wave configuration that leads to upconversion coupling is mainly governed by the ordering of the "group velocities" (50). In a two-dimensional geometry, radiation can be generated from the collision of two upper-hybrid waves in a cold plasma only when the plasma waves are in the first and second (or by symmetry, in the third and fourth) quadrants with respect to the background magnetic field $\mathbf{B} = B_0\mathbf{e}_z$ (see Figure 8). Furthermore, the optimal coupling configuration (for which the threshold for pump depletion or absolute instability is a minimum) is attained when the electrostatic wave vectors, $\mathbf{k}_{L1}$ and $\mathbf{k}_{L2}$, are almost field-aligned and have opposite parallel components ($k_{L1\parallel} = -k_{L2\parallel} \gg k_{L1,2\perp}$). However, the electrostatic upper-hybrid waves excited in our temperature anisotropy instability (section 3.2) are mostly propagating orthogonally to the magnetic field ($\theta = 80°$ or $100°$). We will discuss in the following how the plasma waves can arrive at the resonance coupling region

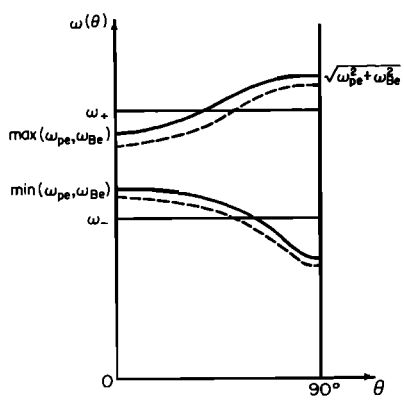

Fig. 9. Eigenfrequencies of longitudinal (es) plasma oscillations as functions of the propagation angle θ in a magnetized plasma. The solid and dashed lines refer to the dispersion curves corresponding to higher and lower plasma densities.

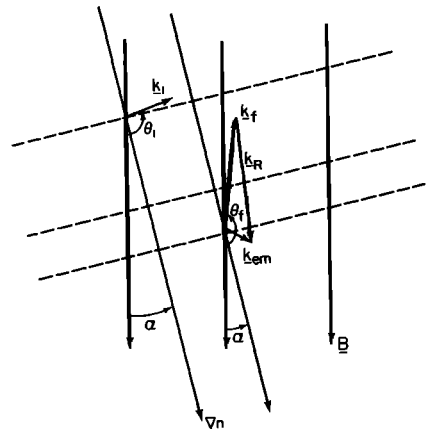

Fig. 10. The electrostatic waves (k_t, θ_t) generated at $\omega_p/\Omega_e = 2.45$ are convected into the density gradient. The waves are reflected at the critical layer where $\omega_p = \omega_L$. At $\omega_p/\Omega_e = 2.6410$, the resonance conditions and the optimal coupling configuration are satisfied so that electromagnetic waves are produced by nonlinear interactions of incident and reflected waves.

via propagation effects. The simultaneous satisfaction of (50) and the respective dispersion relations (45, 46) of the interacting waves as well as the wave resonance conditions, implies that only limited combinations of ω_{Lj} and $\mathbf{k}_{Lj}$ ($j = 1, 2$) can lead to the production of electromagnetic waves (ω_{em}, $\mathbf{k}_{em}$). Hence, the resultant radiation is expected to be highly beamed.

Once the plasma waves are excited, their frequencies remain constant as they propagate. Their wavelengths, however, may change according to the gentle (WKB) variation of the dielectric properties of the plasma. Refraction and reflection of the waves can then help turning the waves into the resonance coupling configuration. The change in wave number (wavelength) of a wave in a slowly varying medium, as we will see, can be described by Snell's law.

We notice that within a given region of the plasma (ω_p, Ω_e), $|\mathbf{k}_{em}|$ is uniquely defined when $\omega_{em}(=\omega_{L1} + \omega_{L2})$ and θ_{em} are known. The frequencies of the electrostatic waves are determined by their wave normal angles (45). Hence, it is important to note that once the electrostatic wave frequencies (ω_{L1}, ω_{L2}) and the electromagnetic wave normal angle (θ_{em}) are determined, the triad of the wave vectors satisfying the k-matching condition (40) is fixed. The remaining question then is whether via propagation effects, such a coupling triad of waves can be found.

We consider next the interaction of two upper hybrid branch waves generated by the temperature anisotropy instability discussed in section 3.2. For simplicity, we only consider the collision of two waves in the fastest growing mode $\omega/\Omega_e = 2.6413$ and $kc/\Omega_e = 51$, excited at $\theta = 100°$ in a region where $\omega_p/\Omega_e = 2.45$. According to the dispersion relation (45) of the electrostatic waves (Figure 9), an upper hybrid branch wave of frequency $\omega_L = \omega_+$ becomes more field aligned, i.e., corresponding to the optimal coupling configuration [*Fung*, 1985*b*] when it propagates into a denser medium [*Roux and Pellat*, 1979]. In addition, refraction causes the wave number to increase as the backward propagating ($v_{pz}v_{gz} < 0$) upper hybrid wave becomes more and more aligned with the background magnetic field (Figure 10). This can be seen by considering

TABLE 1*a*. Possible Coupling Configurations Attainable by Upper Hybrid Waves Generated at $\omega_p/\Omega_e = 2.45$, as they Propagate Into the Region Where $\omega_p/\Omega_e = 2.641$

ω_p/Ω_e	θ_1	θ_2	θ_{em}	ω_1/Ω_e	ω_2/Ω_e	ω_{em}/Ω_e	k_{L1}	k_{L2}	k_{em}
				For R-X Mode					
2.6410	2.1	177.3	90.0	2.6413	2.6415	5.283	53.726	53.749	4.537
2.6410	2.1	177.3	91.0	2.6413	2.6415	5.283	53.670	53.773	4.537
				For L-O Mode					
2.6410	2.1	177.3	90.0	2.6413	2.6415	5.283	54.179	54.204	4.575
2.6410	2.1	177.3	91.0	2.6413	2.6415	5.283	54.128	54.233	4.575
2.6410	2.1	177.3	92.0	2.6413	2.6415	5.283	54.064	54.249	4.576

Snell's law, which can be stated simply as

$$k_i \sin(\theta_i - \alpha) = k_f \sin(\theta_f - \alpha) \tag{57}$$

where α, here, is the angle between the ambient magnetic field and the direction of the density gradient; θ_i and θ_f are the wave normal angles before and after refraction; k_i and k_f are the corresponding wave numbers. Therefore, as the wave becomes field-aligned, we have $\alpha < \pi/2 < \theta_i < \theta_f$ (Figure 10) and thus $k_f > k_i$. Actual couplings are not possible unless the wave number k_f is larger than the wave number excited by the plasma instability. In our example, we require that $k_f > k_i = 51\ \Omega_e/c$.

Solving (57) for α, we have

$$\tan\alpha = \frac{(k_f/k_i \sin\theta_f - \sin\theta_i)}{(k_f/k_i \cos\theta_f - \cos\theta_i)} \tag{58}$$

It is clear that when the density gradient and magnetic field are parallel ($\alpha = 0$) or perpendicular ($\alpha = \pm\pi/2$) to each other, the numerator or denominator of (58) vanishes as expected. Equation (58) allows us to ascertain the angle between the density gradient and the ambient magnetic field in the plasma which will facilitate the coupling.

In order to complete the vector sum of the three wave vectors according to (40), we need two almost oppositely propagating electrostatic waves (see Figures 8 and 10). They can be furnished by the reflection of the incident wave (ω_{L1}, $k_f = k_{L1}$). As the primary wave propagates into the density gradient [recall that upper hybrid waves are backward travelling waves, $v_{phz}v_{gz} < 0$] and reaches the critical layer where $\omega_{L1} = \omega_p$, plasma oscillations are set up along the direction of the ambient magnetic field. Beyond this layer, however, the local plasma frequencies are higher than the wave frequency and the wave becomes evanescent. Absorption or reflection of the wave may occur depending on the strengths of the damping processes [*Stix*, 1962]. As long as the plasma remains cold ($v_e \ll \omega/k_z$, $k\lambda_D \ll 1$), Landau damping is negligible. Cyclotron damping is also unimportant when both v_e and $k_\perp$ are small (i.e., $k_\perp\rho_e \to 0$). At the critical layer, $k_{L1z}(=k_f)$ can be obtained by setting $\theta_f = 180°$ in (57). With $\omega_{L1}/\Omega_e = 2.6413$ and $T_e = 25$ eV (Figure 5), we have $\omega/k_{1z} \simeq 7v_e$ and $k_{1z}\lambda_D = 0.15$. Thus the cold plasma approximation is reasonably well satisfied. As the group velocities of electrostatic waves vanish at the critical layer ($\theta = 0$), waves must be reflected instead of absorbed [*Fung*, 1985*b*].

In our model, the electrostatic waves generated at $\theta_i = 100°$ to the magnetic field propagate toward the magnetic equator and into regions of higher ω_p/Ω_e. The incident and reflected waves then collide to produce electromagnetic waves (see Figures 10 and 12). All possible coupling configurations that satisfy simultaneously the coupling conditions defined in section 5.1 are listed in Table 1*a*. The plasma region in which these couplings occur is where $\omega_p/\Omega_e = 2.641$ (i.e., $\omega_{L1,2} \gtrsim \omega_p$). We see that these configurations are close to the optimal coupling configuration. Namely, the electrostatic waves are almost field aligned and propagating opposite to each other; whereas the electromagnetic waves are beamed close to perpendicular propagation. We should mention that upconversion coupling would not occur in regions of lower densities ($2.45 < \omega_p/\Omega_e \lesssim 2.641$) because the appropriate wave numbers of the electrostatic waves required for couplings are smaller than $51\ \Omega_e/c$ (k_i), conflicting with Snell's law. From the allowed coupling configurations (Table 1*a*), we have $\theta_f = 177.3°$ and $k_f c/\Omega_e = 53.7$. Thus (58) implies that if there is an inclination of 47° (−47°) between the density gradient and magnetic field in the northern (southern) hemisphere, upconversion interactions of two oppositely propagating upper hybrid waves can lead to the generation of radiation that is beamed to within two degrees from the normal to the magnetic field. (Note that we have adopted the convention that angles measured counterclockwise from the magnetic field are positive.) This is illustrated in Figure 10.

With the magnetic field pointing southward (down), Figure 10 implies that the density gradients of the nKOM source regions (both northern and southern components) must be pointing toward the magnetic equator and away from the cold torus center. This may seem to contradict with the expected directions of the density gradients in the main part of the Io plasma torus (i.e., radially inward toward the center of the cold torus as expected from Figure 2). However, as the outer portion of the Io plasma torus is known to be distended, the direction of the local density gradient normal to the magnetic field can indeed be reversed if there is a relative increase of

TABLE 1*b*. Q Values Associated With the Coupling Configurations in Table 1*a*

Q_{L1}	Q_{L2}	Q_{em}
	For R-X Mode	
0.0455	0.0454	2.28
0.0723	0.0379	3.01
	For L-O Mode	
1.57×10^{-5}	1.57×10^{-5}	1.01
6.61×10^{-3}	4.68×10^{-3}	0.297
1.62×10^{-2}	6.86×10^{-3}	0.662

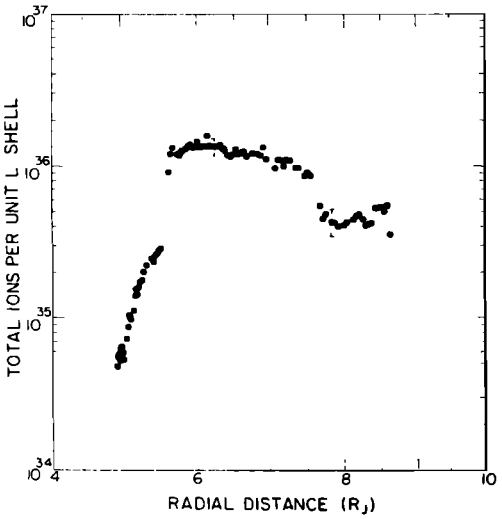

Fig. 11. Radial profile of the total number of ions per unit L shell constructed from in-situ plasma measurements, assuming a dipole magnetic field and a simple exponential scale height distribution for the ions along the field lines. The uncertainties due to thermal-model dependencies are shown by the vertical bars [*Bagenal and Sullivan*, 1981].

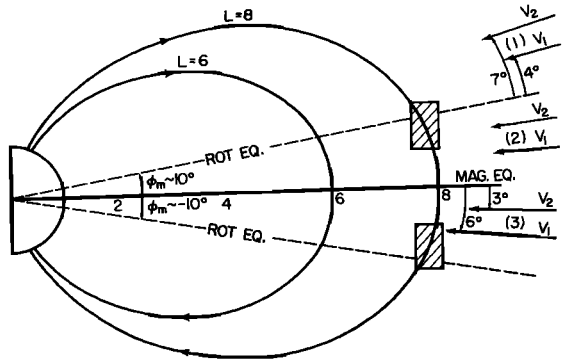

Fig. 12. Meridional projection of the Jovian inner magnetosphere. The shaded regions are the proposed locations of the northern and southern components of then nKOM source. Also shown are the relative positions of the Voyager spacecraft. Positions 1 and 3 are the maximum excursions of the spacecraft in magnetic latitudes. Position 2 is when the Jovigraphic and magnetic equators coincide.

plasma density at radial distances beyond about 7.8 R_J. Shown in Figure 11 is a radial profile of the total number of ions per unit L shell constructed from in-situ plasma measurement [*Bagenal and Sullivan*, 1981]. We see that there is strong indication of an increase in ion density for $R \gtrsim 7.8\ R_J$. Similar behavior for the electron profile is expected due to quasineutrality. This feature naturally provides the proper orientation of the density gradient with respect to the magnetic field for the coupling of two upper hybrid branch waves.

We propose then that nonlinear coupling of upper hybrid branch waves generated by plasma instability such as that due to temperature anisotropy (section 3.2) can lead to the emission of the Jovian nKOM. A Jovian meridional plane projection of the source location of nKOM (shaded areas) is shown in Figure 12. Plasma waves excited by the instability propagate toward regions of higher ω_p/Ω_e and become more field-aligned. They are then reflected at the critical layers. The interactions between the incoming and reflected waves can then produce electromagnetic waves that are beamed normal to the magnetic field. This situation is depicted in Figure 10.

Due to the inclination ($\sim 10°$) between the rotational and magnetic axes of Jupiter, both Voyager 1 and 2 spacecraft [having inbound Jovigraphic latitudes of $+4°$ and $+7°$, respectively) oscillate in magnetic latitudes between positions 1 and 3 as shown in Figure 12. When the rotational and magnetic equators coincide, the spacecraft are in position 2. It is apparent that when the spacecraft are in the southern magnetic hemisphere (position 3), the radiation observable by the spacecraft is characterized by $\mathbf{k}_{em} \cdot \mathbf{B}_0 < 0$; whereas in the northern magnetic hemisphere, $\mathbf{k}_{em} \cdot \mathbf{B}_0 > 0$. As we will see in the next section these quantities are crucial for relating the observed polarization of the radiation to the mode of propagation. Since no nKOM events are detectable by Voyager 1 at position 1, the width of the total radiation beam must be less than about 4°, consistent with Table 1*a*.

6. Polarization and Power

The net polarization of the radiation depends on the dominant mode of propagation generated (*R-X* or *L-O* mode). In *R-X* mode, an electromagnetic wave propagating in the direction of the magnetic field has its electric field rotating in the direction of gyration of electrons (right-handed). The electric vector of an *L-O* mode wave propagating along a magnetic field rotates according to ion gyration (left-handed).

Observationally, however, the sense of polarization of radiation is defined according to the rotation of the electric vector about the wave propagation vector $\mathbf{k}_{em}$. For an approaching wave, a counterclockwise rotating electric field is right-handed polarized (RH); a clockwise rotating electric field is left-handed polarized (LH). Thus the mode of propagation of the observed radiation can be determined when both the sense of polarization and the relative orientation between the wave vector and the background magnetic field in the source region are known. As the net polarization of nKOM is observed to be left-handed in the northern (magnetic) hemisphere and right-handed in the southern hemisphere, and $\mathbf{k}_{em} \cdot \mathbf{B}_0 > 0$ in the north and $\mathbf{k}_{em} \cdot \mathbf{B}_0 < 0$ in the south, the nKOM must be emitted predominantly in the *L-O* mode.

In Table 1*b*, we have listed the Q values (see (54) and (56)) corresponding to the couplings of two upper hybrid waves (Table 1*a*). The pump depletion threshold can be calculated by using (53); then we have (56)

$$\varepsilon_{th} \simeq \frac{\pi}{2QL} \tag{59}$$

It is apparent that both Q_{L1} and Q_{L2} for the generation of *L-O* mode are smaller than they are for *R-X* mode; and the corresponding Q_{em} for *L-O* mode is also smaller than that for the *R-X* mode. Hence, the generation of *L-O* mode requires a stronger pump wave amplitude. Given a sufficiently strong electrostatic pump wave level, the *L-O* mode is the dominant mode to be emitted. If we take the pulse length L to be 0.1 L_n, where $L_n \simeq 1\ R_J$ is the density scale height of the warm torus [*Bagenal and Sullivan*, 1981], $Q_{L1,2} \simeq 6 \times 10^{-3}$ for *L-O* mode and $Q_{L1,2} \simeq 4 \times 10^{-2}$ for *R-X* mode (Table 1*b*), then the pump depletion threshold for the generation of *L-O* mode is $\varepsilon_{th} \sim 10$ mV/m and that for *R-X* mode is $\varepsilon_{th} \sim 1.3$ mV/m.

Observationally, the $(n + 1/2)\Omega_e$ waves are amongst the strongest electrostatic waves measured in the inner Jovian magnetosphere (Figure 4*d*). Their amplitudes do reach as high as a few millivolts per meter to 10 mV/m [*Kurth et al.*, 1980*a*; *Gurnett and Scarf*, 1983]. We can, therefore, expect that elec-

tromagnetic waves in both *L-O* and *R-X* modes can be nonlinearly excited in the outer periphery of the Io plasma torus.

The radiation flux density F_{obs} observed at a distance D from the source region is given by

$$F_{obs} = I_\nu \frac{A_s}{D^2} \tag{60}$$

where A_s is the radiation source area and I_ν is the specific intensity [*Bekefi*, 1966] of the radiation at frequency ν, bandwidth $\Delta\nu$, radiation beam solid angle subtended at the source $\Delta\Omega$, radiation energy density W (23) and group (energy propagation) velocity v_g (20); I_ν is given by

$$I_\nu = \frac{W v_g}{\Delta\nu \Delta\Omega} \tag{61}$$

When the electrostatic pump wave levels are high enough to cause pump depletion ($\varepsilon \sim \varepsilon_{th}$), solitons are transferred into the high frequency electromagnetic waves (see section 5.2). If the radiation level is limited by the subsequent decay of the electromagnetic wave back into the electrostatic waves, the resulting radiation then saturates at the corresponding pump-depletion threshold level which is again given by (59) with $Q = Q_{em}$. We note here that Q_{em} is calculated self-consistently with $Q_{L1,2}$; the radiation saturation level obtained in this fashion is valid only when the electrostatic pump waves are sufficiently strong to cause pump-depletion in generating the electromagnetic wave. The more complete description of the relation between the "areas" of pump and daughter waves must be used when more general situation is considered [*Fung*, 1985*b*].

If we assume that the planetary dipole magnetic field in the Io plasma torus region is essentially perpendicular to the magnetic equator, we can take the radiation emitted from every point in the source region to be confined to a beamlet of 1 degree radius (Table 1*a*). This corresponds to a beamlet solid angle of $\Delta\Omega = 9.6 \times 10^{-4}$ steradian. Taking $\Delta\nu = 40$ kHz, $v_g \simeq c$, $Q_{em} \simeq 0.3$ for *L-O* mode and 3.0 for *R-X* mode (Table 1*b*), $A_s \simeq 10^2 L^2$ ($L \sim 0.1$ R_J), we can estimate the flux density F_{obs} observed at a distance of 4 AU to be 4.75×10^{-22} Wm^{-2} Hz^{-1} for the *R-X* mode, and as high as 4.75×10^{-20} Wm^{-2} Hz^{-1} for the *L-O* mode. This is in good agreement with the observations (Figure 1).

7. Discussion

We presented a model for the generation of the narrowband Jovian kilometric radiation (nKOM). Using the coherent nonlinear three-wave interaction formalism, we have found that upconversion of two upper hybrid branch electrostatic waves can produce electromagnetic radiation that can account for the observed radio emission. The model is found to be in good agreement, both qualitatively and quantitatively, with the observations.

The presence of electrostatic $(n + 1/2)\Omega_e$ waves in the Io plasma torus [*Kurth et al.*, 1980*a*; *Birmingham et al.*, 1981] naturally provides the pump waves needed for the coupling. In section 3.2, we examined a possible excitation mechanism for these plasma waves. We found that in a cold plasma mixed with a small component ($n_H/n_c \ll 1$) of hot electrons, upper-hybrid branch ($\omega_p \lesssim \omega_L \lesssim \omega_{UH}$) electrostatic waves can be excited if there exists a temperature anisotropy ($T_\perp > T_\parallel$) in the hot electrons. If the plasma parameters (ω_p, Ω_e) have small spatial variations (WKB-like), then in the cold plasma limit the plasma waves are refracted as they propagate. Their wave vectors turn toward alignment with the background magnetic field as the ratio ω_p/Ω_e increases (Figure 9) while their wavelengths decrease according to Snell's law (57). If the plasma remains cold ($v_e \ll \omega_L/k$ and $k\lambda_D \ll 1$) and collisionless, the plasma waves are reflected upon reaching the critical layer ($\omega_L = \omega_p$). The interactions between the incoming and reflected electrostatic waves generate electromagnetic radiations in both *L-O* and *R-X* modes, beamed perpendicularly to the ambient magnetic field.

The nKOM source location is fairly well determined. From the relative drifts of the nKOM events in system III longitudes, *Kaiser and Desch* [1980] have determined that the nKOM source is situated in the outer periphery of the Io plasma torus, where the local plasma characteristic frequencies (ω_p, Ω_e) can support waves of frequencies comparable to the nKOM frequencies. Direct plasma measurements made at 7.5–8 R_J in the plasma torus also confirmed the deviation from corotation at this outer portion of the plasma torus [*Bagenal and Sullivan*, 1981]. Our study concluded in sections 2 and 3 that a reasonable nKOM source location is the region of the plasma torus near 8 R_J where the plasma parameters are given by $2.3 < \omega_p/\Omega_e < 2.7$. Two such regions exist in the torus, one in each magnetic hemisphere at magnetic latitudes $\phi_m \sim \pm 10°$. Due to the inclination between the magnetic (centrifugal) and Jovigraphic equators of Jupiter by about 10°, the magnetic latitudes of the Voyager spacecraft (which have Jovigraphic latitudes of +4° and +7° for V1 and V2, respectively) vary between the range of $-6° \lesssim \phi_m \lesssim +17°$. Therefore, except perhaps when the north magnetic pole is tipped toward the spacecraft, the nKOM radiation detected in the northern magnetic hemisphere is characterized by $\mathbf{k}_{em} \cdot \mathbf{B}_0 > 0$ while when the spacecraft are in the southern (magnetic) hemisphere, the detected radiation is characterized by $\mathbf{k}_{em} \cdot \mathbf{B}_0 < 0$ (Figure 12). For *L-O* mode radiation, the polarization observed north of the neutral sheet would then be left handed; in the southern hemisphere it would be right handed. This can account for the polarization reversal of nKOM events during current sheet crossings [*Kaiser and Desch*, 1980, 1984]. When the northern magnetic pole is tilted toward the spacecraft, the (northern) source of nKOM is situated at a lower latitude ($\phi_m \sim 10°$) than the detector ($\phi_m \sim -17°$ for *V2* and $\phi_m \sim 14°$ for *V1*). During these times, however, the emissions of bKOM are strongest [*Desch and Kaiser*, 1980] and any nKOM event would be overwhelmed by the stronger bKOM event. This is consistent with the fact that nKOM events are typically seen between bKOM events [*Desch and Kaiser*, 1980; *Carr et al.*, 1983].

Assuming that the radiation saturates at the corresponding pump depletion level, the expected *L-O* mode flux density normalized to an observing distance of 4 AU can be as high as 4.75×10^{-20} Wm^{-2} Hz^{-1}, comparable to the strongest observed value (Figure 1). This implies that depletions of the electrostatic pumps must occur; and the conversion of electrostatic wave energy into radiation is close to complete. The level of electrostatic waves required is about 10 mV/m.

A remarkable feature of the nKOM is that the emission can go off for a period of time (say, a few planetary rotations) and reappear without any phase-lag in the nKOM occurrence pattern [*Kaiser and Desch*, 1980]. This indicates that the source region remains coherent at all times. We have seen in Section 5.2 that the occurrence of coupling of the electrostatic plasma waves relies on the presence of a density gradient. The orientation of the density gradient with respect to the magnetic field

effectively determines the location of the resonance region and the beaming angles of the resultant radiation. Figure 11 strongly suggests that the proper orientation of the local density gradient exists near the source region of nKOM ($7.5\ R_J < R < 9\ R_J$). Temporary "blackouts" of the nKOM can result if the "reversed" density gradient has a slow time variation.

In our model, we relied on the propagation effects of the electrostatic waves in a slightly inhomogeneous plasma to achieve the proper coupling configuration. However, the region of interaction was regarded as sufficiently small ($L < 0.1\ L_n$) so that it is essentially homogeneous. We, therefore, attribute the observed bandwidth ($\Delta\nu \sim 40$ to 80 kHz) of the nKOM to the large scale inhomogeneity within the Io plasma torus. Although narrow-band emission is expected from a coherent interaction, when density or magnetic gradient (preserving WKB) exists in the plasma, the wave resonance conditions can only be satisfied locally (see section 3). If such local resonances are satisfied over an extended region of the plasma, broadband emission may result. Alternatively, when the plasma parameters (ω_p, Ω_e) vary sufficiently rapidly (still remaining WKB for wave propagation), the eigenfrequencies of the electrostatic waves would have finite bandwidths. In this case, the resonances between the central frequencies and the corresponding neighboring frequencies in the interacting wave packets will result in broadband emission via incoherent interactions [*Hasegawa*, 1975]. Therefore, nonlinear wave-wave interactions may also be responsible for the emission of the bKOM [*Desch and Kaiser*, 1980]. An extension of our theory to the bKOM will be considered in a separate paper.

Acknowledgments. We thank M. L. Kaiser and M. D. Desch of NASA Goddard Space Flight Center for providing their planetary radio astronomy (PRA) data from the Voyager encounters with Jupiter. Their assistance and clarification in our interpretation of the data were invaluable. Important discussions with M. Goldstein and L. Vlahos are also acknowledged. The work in this paper was supported (S.F.F. and K.P.) by NASA grant NAGW-81 and partially (S.F.F.) by NASA contract NAS5-29312. Computations were partially supported by the Computer Science Center of the University of Maryland.

REFERENCES

Akhiezer, A. I., I. A. Akhiezer, R. V. Polovin, A. G. Sitenko, and K. N. Stepanov, *Plasma Electrodynamics*, vol. 1, Pergamon, New York, 1975.

Allis, W. P., S. J. Buchsbaum, and A. Bers, *Waves in Anisotropic Plasmas*, MIT Press, Cambridge, Mass., 1962.

Ashour-Abdalla, M., C. F. Kennel, and D. D. Sentman, Magnetospheric multi-harmonic instabilities, in *Astrophysics and Space Science Book Series*, edited by P. J. Palmadesso and K. Papadopoulos, D. Reidel, Hingham, Mass., 1979.

Bagenal, F., and J. D. Sullivan, Direct plasma measurements in the Io torus and inner magnetosphere of Jupiter, *J. Geophys. Res.*, *86*, 8447–8466, 1981.

Bekefi, G., *Radiation Processes in Plasmas*, John Wiley, New York, 1966.

Birmingham, T. J., J. K. Alexander, M. D. Desch, R. F. Hubbard, and B. M. Pedersen, Observations of electron gyroharmonic waves and the structure of the Io torus, *J. Geophys. Res.*, *86*, 8497–8507, 1981.

Burke, B. F., and K. L. Franklin, Observations of a variable radio source associated with the planet Jupiter, *J. Geophys. Res.*, *60*, 213–217, 1955.

Carr, T. D., and M. D. Desch, Recent decametric and hectometric observations of Jupiter, in *Jupiter*, edited by T. Gehrels, pp. 693–735, University of Arizona Press, Tucson, Ariz., 1976.

Carr, T. D., G. W. Brown, A. G. Smith, C. S. Higgins, and H. Bollhagen, Spectral distribution of the decametric radiation from Jupiter in 1961, *Astrophys. J.*, *140*, 778–795, 1964.

Carr, T. D., M. D. Desch, and J. K. Alexander, Phenomenology of magnetospheric radio emission, in *Physics of the Jovian Magnetosphere*, edited by A. J. Dessler, Cambridge University Press, New York, 1983.

Daigne, G., and Y. Leblanc, Narrow-band Jovian kilometric radiation: Occurrence, polarization and rotation period, *J. Geophys. Res.*, *91*, 7961–7969, 1986.

Davidson, R. C., *Method in Nonlinear Plasma Theory*, Academic, Orlando, Fla., 1972.

Desch, M. D., and M. L. Kaiser, The occurrence rate, polarization character and intensity of broadband Jovian kilometric radiation, *J. Geophys. Res.*, *85*, 4248–5256, 1980.

Dory, R. A., G. E. Guest, and E. G. Harris, Unstable electrostatic plasma waves propagating perpendicular to a magnetic field, *Phys. Rev. Lett.*, *14*, 131, 1965.

Ellis, G. R. A., The decametric radio emission of Jupiter, *Radio Sci.*, *69D*, 1513–1530, 1965.

Fung, S. F., Emission of narrow-band Jovian kilometric radiation, *eos Trans. AGU*, *66*, 342, 1985*a*.

Fung, S. F., Radiation from nonlinear coupling of plasma waves, Ph.D. dissertation, Astron. Program, Univ. of Md., College Park, 1985*b*.

Goldstein, M. L., R. R. Sharma, M. Ben-Ari, A. Eviatar, and K. Papadopoulos, A theory of Jovian decameter radiation, *J. Geophys. Res.*, *88*, 792–802, 1983.

Green, J. L., and D. A. Gurnett, Ray tracing of Jovian kilometric radiation, *Geophys. Res. Lett.*, *7*, 65–68, 1980.

Gurnett, D. A., and F. L. Scarf, Plasma waves in the Jovian magnetosphere, in *Physics of the Jovian Magnetosphere*, edited by A. J. Dessler, Cambridge University Press, New York, 1983.

Harris, E. G., Unstable plasma oscillations in a magnetic field, *Phys. Rev. Lett.*, *2*, 34, 1959.

Hasegawa, A., *Plasma Instabilities and Nonlinear Effects*, Springer-Verlag, New York, 1975.

Hill, T. W., Inertial limit to corotation, *J. Geophys. Res.*, *84*, 6554, 1979.

Hill, T. W., Corotation lag in Jupiter's magnetosphere: A comparison of observation and theory, *Science*, *207*, 301–302, 1980.

Hubbard, R. F., and T. J. Birmingham, Electrostatic emissions between electron gyroharmonics in the outer magnetosphere, *J. Geophys. Res.*, *83*, 4837–4850, 1978.

Kaiser, M. L., and M. D. Desch, Narrow-band Jovian kilometric radiation: A new radio component, *Geophys. Res. Lett.*, *7*, 389–392, 1980.

Kaiser, M. L., and M. D. Desch, Radio emission from the planets Earth, Jupiter, and Saturn, *Rev. Space Phys.*, *22*, 373–384, 1984.

Kaup, D. J., A. Reiman, and A. Bers, Space-time evolution of nonlinear three-wave interactions, I, Interaction in a homogeneous medium, *Rev. Mod. Phys.*, *51*, 275–309, 1979.

Kurth, W. S., D. D. Barbosa, D. A. Gurnett, and F. L. Scarf, Electrostatic waves in the Jovian magnetosphere, *Geophys. Res. Lett.*, *7*, 57–60, 1980*a*.

Kurth, W. S., L. A. Frank, M. Ashour-Abdalla, D. A. Gurnett, and B. G. Burek, Observations of a free-energy source for intense electrostatic waves, *Geophys. Res. Lett.*, *7*, 293–296, 1980*b*.

Landau, L. D., and E. M. Lifshitz, *Electrodynamics of Continuous Media*, Pergamon, New York, 1960.

McClain, E. F., and R. M. Sloanaker, Preliminary observations at 10 cm wavelength using the NRL 84-Foot radio telescope, in *Proceedings of IAU Symposium No. 9, URSI Symposium No. 1*, edited by R. Bracewell, pp. 61–68, Stanford University Press, Stanford, Calif., 1959.

Merzbacher, E., *Quantum Mechanics*, John Wiley, New York, 1970.

Mikhailovskii, A. B., *Theory of Plasma Instabilities*, Consultants Bureau, New York, 1974.

Rosenbluth, M. N., Parametric instabilities in inhomogeneous media, *Phys. Rev. Lett.*, *29*, 565–567, 1972.

Roux, A., and R. Pellat, Coherent generation of the auroral kilometric radiation by nonlinear beatings between electrostatic waves, *J. Geophys. Res.*, *84*, 5189–5198, 1979.

Scarf, F. L., D. A. Gurnett, and W. S. Kurth, Measurement of plasma wave spectra in Jupiter's magnetosphere, *J. Geophys. Res.*, *86*, 8181–8198, 1981.

Scudder, J. D., E. C. Sittler, and H. S. Bridge, A survey of the plasma electron environment of Jupiter: A view from Voyager, *J. Geophys. Res.*, *86*, 8157–8179, 1981.

Siscoe, G. L., A. Eviatar, R. M. Thorne, and J. D. Richardson, Ring current impoundment of the Io plasma torus, *J. Geophys. Res.*, *86*, 8480–8484, 1981.

Sloanaker, R. M., Apparent temperature of Jupiter at a wavelength of 10 cm, *Astron. J.*, *64*, 346, 1959.

Stix, T. H., *The Theory of Plasma Waves*, McGraw-Hill, New York, 1962.

Urrutia, J. M., and R. L. Stenzel, Observations of odd-half cyclotron harmonic emissions in a shell-Maxwellian laboratory plasma, *J. Geophys. Res.*, *88*, 7086–7094, 1983.

Warwick, J. W., et al., Voyager 1 planetary radio astronomy observations near Jupiter, *Science*, *204*, 995–998, 1979*a*.

Warwick, J. W., et al., Planetary radio astronomy observations from Voyager 2 near Jupiter, *Science*, *206*, 991–995, 1979*b*.

Zabriskie, F. R., Low-frequency radio emission from Jupiter, *Astron. J.*, *75*, 1045–1051, 1970.

Zakharov, V. E., and S. V. Manakov, The theory of resonance interaction of wave packets in nonlinear media, *Sov. Phys. JETP*, *42*, 842–850, 1976.

S. F. Fung, NASA Goddard Space Flight Center, Code 696, Greenbelt, MD 20771.

K. Papadopoulos, Astronomy Program, University of Maryland, College Park, MD 20742.

(Received September 12, 1986;
revised April 15, 1987;
accepted April 30, 1987.)